ENERGETICS OF SIMULATED HCDA BUBBLE EXPANSIONS: SOME POTENTIAL ATTENUATION MECHANISMS

R. J. TOBIN

SRI International
333 Ravenswood Ave., Menlo Park, California 94025, U.S.A.

D. J. CAGLIOSTRO

Los Alamos Scientific Laboratory, Los Alamos, NM 87545, U.S.A.

Mail proofs to: R. J. Tobin
Research Engineer
Engineering Mechanics Department
Poulter Laboratory
SRI International
333 Ravenswood Avenue
Menlo Park, CA 94025

ENERGETICS OF SIMULATED HCDA BUBBLE EXPANSIONS: SOME POTENTIAL ATTENUATION MECHANISMS

R. J. Tobin
Poulter Laboratory, SRI International,
Menlo Park, CA 94025, USA

D. J. Cagliostro
Los Alamos Scientific Laboratory,
Los Alamos, NM 87545, USA

Experiments conducted to increase our understanding of the dynamics and thermodynamics of expanding bubbles similar to the core disruptive accident (CDA) bubble in liquid metal fast breeder reactors (LMFBR) are described. The experiments were conducted in a transparent 1/30-scale model of a typical demonstration-size loop-type LMFBR in which water at room temperature simulated the sodium coolant. Nitrogen gas (1450 psia) and flashing water (1160 psia) qualitatively simulated sodium vapor and molten fuel expansions. Three physical mechanisms that may result in attenuation of the work potential of a hypothetical CDA (HCDA) were revealed by the experiments: (1) the pressure gradient existing between the lower core and the bubble within the pool, (2) the hydrodynamic effects of vessel internal structures, and (3) the nonequilibrium flashing process occurring in the lower core. These three mechanisms combine to result in a coolant axial slug kinetic energy that is only 14% of the work potential of the ideal quasi-static nitrogen expansion and only 5% of the work potential of the ideal quasi-static flashing water expansion.

1. Introduction

LMFBR accidents involving core meltdown are considered to have the greatest potential for releasing significant amounts of radioactivity to the environment. Such accidents are called core disruptive accidents (CDAs). If a core meltdown could occur, then theoretically, core material motions and interactions might lead to rapid pressure-generation events that could cause structural damage to the reactor and possible release of radioactive materials.

Realistic predictions of the energetics, or work potential, of hypothetical CDAs (HCDAs) are a concern in the safety analysis of LMFBRs. Predictions are currently based on conservative nonmechanistic assumptions concerning the progression of severe core meltdown accidents. Recently, both experiments and analyses have shown that natural attenuation mechanisms, such as flow around internal structures, may substantially reduce HCDA energetics. The experiments described here were conducted to study the effects of vessel internal structures [1], increase our understanding of the dynamics and thermodynamics of expanding bubbles similar to the CDA bubble in LMFBRs, and aid in developing analytical models for predicting CDA energetics.

Our approach was to simulate the qualitative features of an HCDA bubble expansion in a simple, 1/30-scale model (fig. 1) of the interior of a typical demonstration-size loop-type LMFBR (fig. 2). Included in our model was an upper core structure (UCS) simulating an array of empty

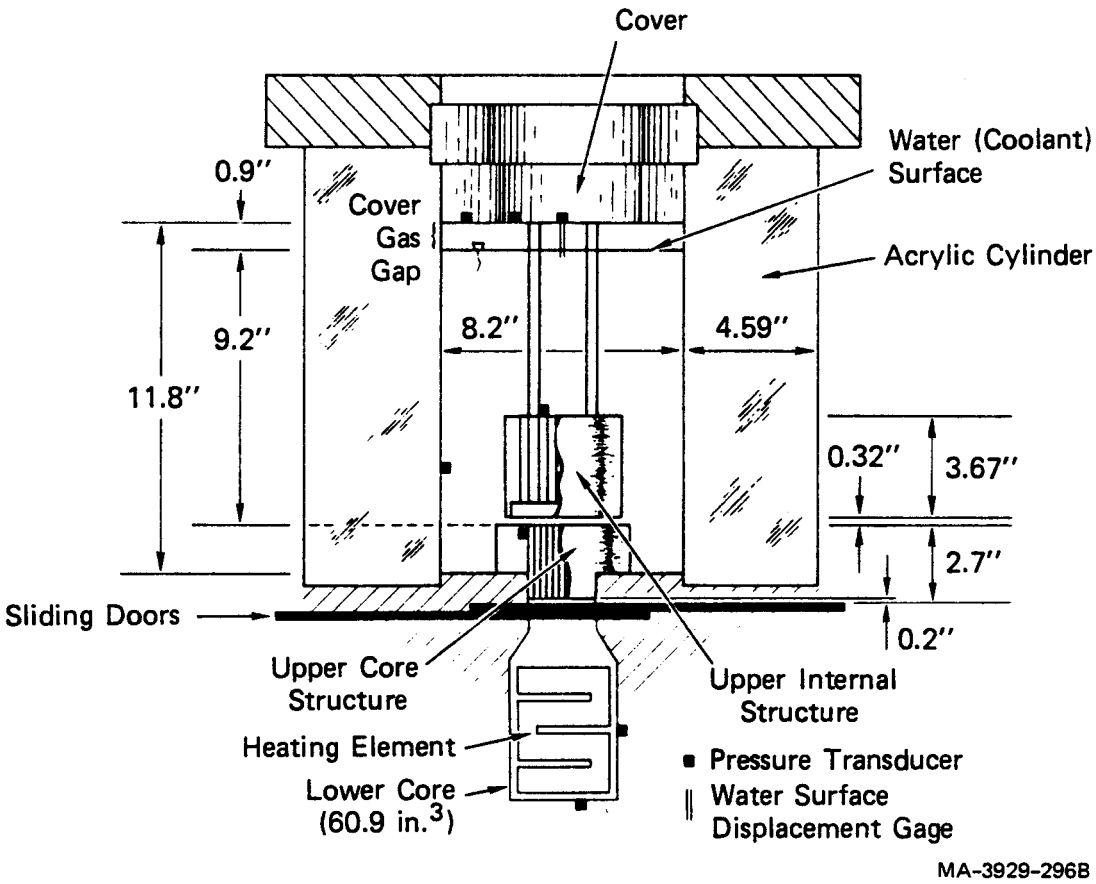

FIGURE 1 1/30-SCALE VESSEL AND INSTRUMENTATION

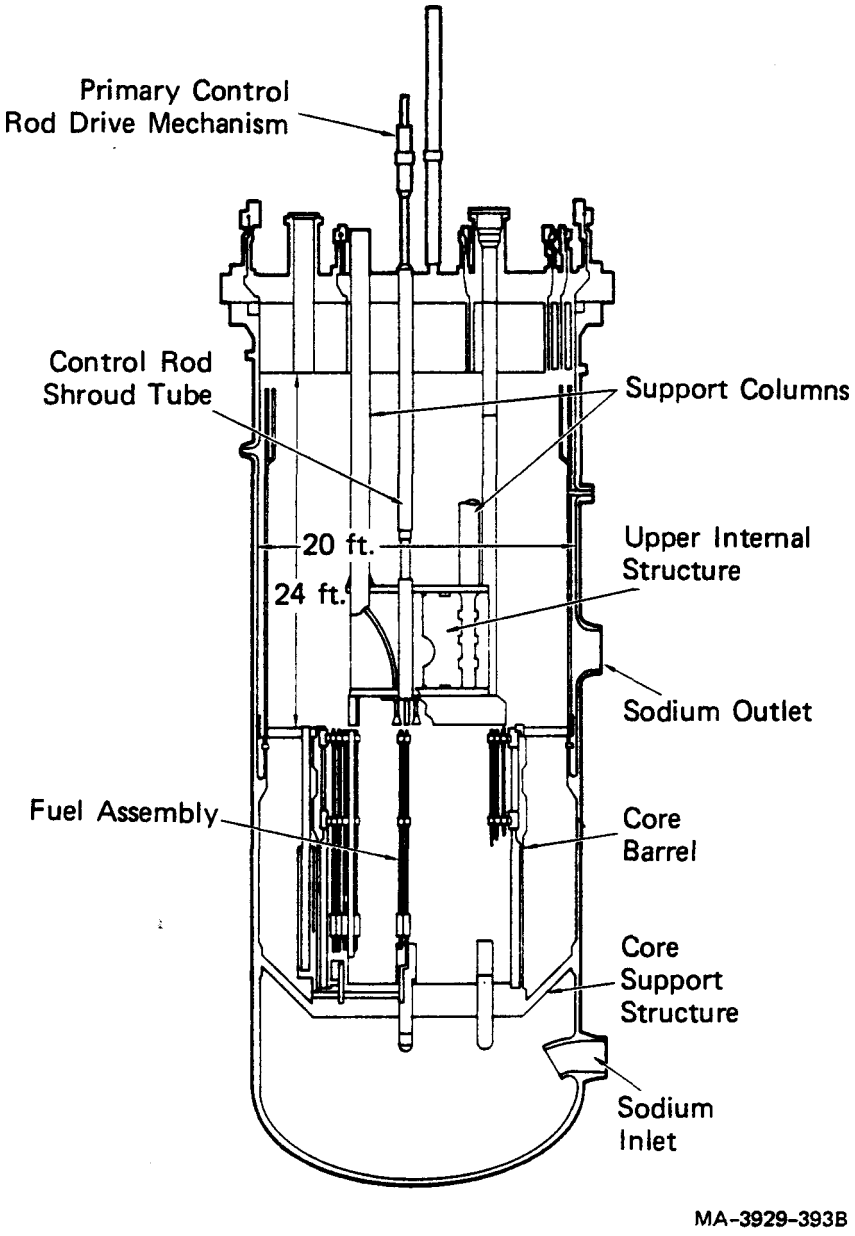

FIGURE 2 TYPICAL DEMONSTRATION SIZE LOOP-TYPE LMFBR

hexcans and an upper internal structure (UIS) simulating the control rod and flow guide. A nitrogen gas (1450 psia) expansion was used to simulate the qualitative features of a sodium vapor expansion. The nitrogen source experiments illuminate the dynamic features of the bubble expansion without the complications of heat transfer and phase change. Flashing water (1160 psia) was used to simulate the qualitative features of a molten fuel expansion. Heat transfer and phase change are present in the flashing water bubble source experiments. The initial pressures were within the range expected for HCDA's. The sodium coolant at low pressure in an LMFBR was simulated in the model by water at room temperature and atmospheric pressure. The bubble expansions and the motion of the coolant simulant were studied using pressure transducers, water surface displacement gages, and high-speed photography.

2. Attenuation Mechanisms

An important objective of any study of HCDA bubble dynamics should be the identification of physical mechanisms that may result in attenuation of thw work potential of an HCDA. Analysis of the experiments discussed here led to identification of three natural attenuating mechanisms: (1) the pressure gradient existing between the lower core and the HCDA bubble within the pool, (2) the hydrodynamic effects of vessel internal structures, and (3) the nonequilibrium flashing process occurring in the lower core. Experiments to study only the attenuating effects of heat transfer between the expanding HCDA source and adjacent solids were conducted earlier by Cagliostro [2] and found to be small relative to heat transfer between the expanding source and the liquid into which it expanded.

3. Experimental Apparatus and Instrumentation

The apparatus used to simulate the qualitative features of an HCDA bubble expansion was a simple 1/30-scale model (fig. 1) of the interior of a typical demonstration-size loop-type LMFBR vessel. Included in our model were upper core and upper internal structures (fig. 3). The diameter of the individual flow channels in the 2.50-inch-long UCS was chosen to closely scale the cross-sectional area of empty subassembly ducts. Similarly, the UIS geometry was linearly scaled to the UIS geometry of a typical demonstration-size loop-type LMFBR. The components in the model were rigid; structural response was not scaled in these experiments. Experiments were performed with and without these structures to clarify their influence on the HCDA bubble expansion.

Sodium coolant was simulated in the model by water at room temperature and atmospheric pressure. The bubble sources simulating the expansion of sodium vapor and molten fuel were contained in the lower core shown in fig. 1. Both high-pressure nitrogen gas (1450 psia and room temperature) and high-pressure flashing water (1160 psia and 563°F) were used as bubble sources. After the appropriate initial conditions were established within the lower core and acrylic vessel, the experiments were initiated at $t = 0$ by detonating an explosive to open the sliding doors, figs. 1 and 4. The flow path between the lower and upper cores began to open at $t = 1.2$ ms and took 230 μs to fully open. The expansion of the gas or flashing liquid contained in the lower core then drove the liquid coolant out of the upper

UPPER INTERNAL STRUCTURE (UIS)

DRILLED HOLES

Number	Diameter
19	0.313"
10	0.332"

FLOW AREA

2.32 $in.^2$

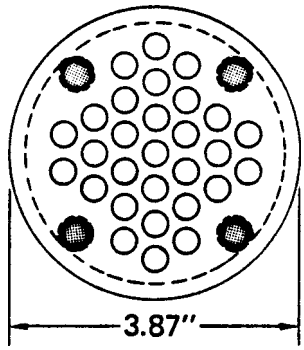

UPPER CORE STRUCTURE (UCS)

DRILLED HOLES

Number	Diameter
139	0.152"

FLOW AREA

2.52 $in.^2$

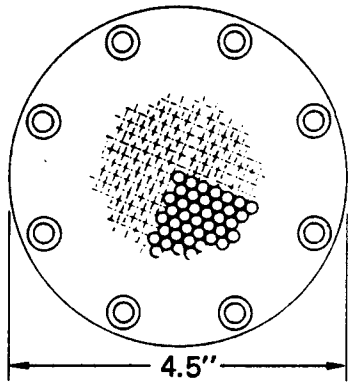

MA-3929-297A

FIGURE 3 TOP VIEW DETAIL OF INTERNAL STRUCTURES

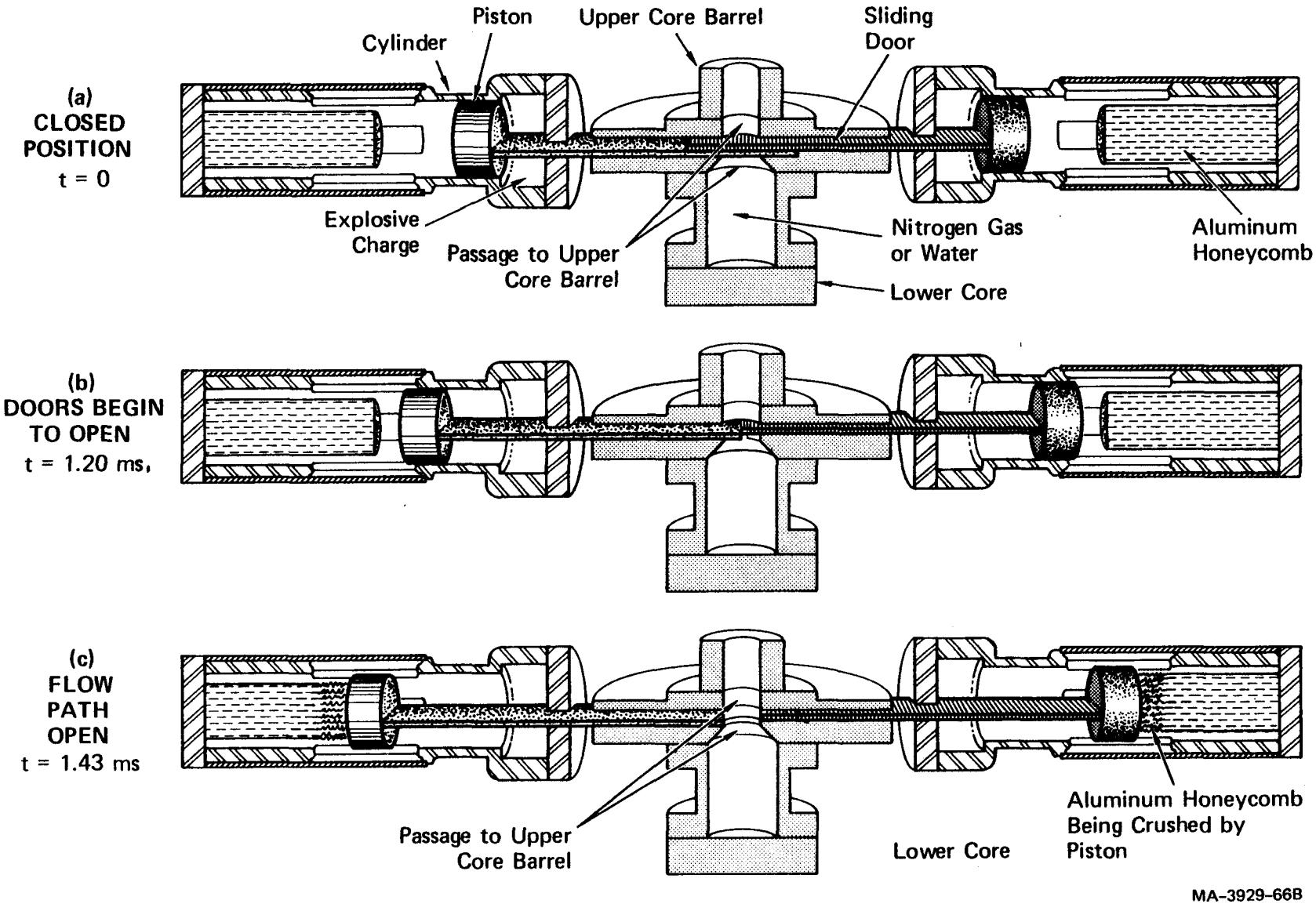

FIGURE 4 SLIDING DOOR OPENING SEQUENCE

core and formed within the coolant pool an expanding bubble, which drove the coolant pool to impact on the vessel cover.

The experiment instrumentation is shown schematically in fig. 1. Pressure gradients within the apparatus were determined from pressure measurements in the lower core, upper core, and within the pool and bubble. Slug impact pressures were measured with pressure transducers located in the vessel cover. The water surface displacement gage measurements were used to determine the expansion history of the bubble source. The entrainment within the expanding bubble was determined by subtracting the volume displacement by the water surface motion from the bubble volume determined by using the bubble outline on the high-speed photographs and assuming a surface of revolution.

Pressures in the lower core, upper core, within the pool and bubble, and at the vessel cover as well as surface displacement of the pool were recorded on both oscillograms and magnetic tape. Quartz piezoelectric pressure transducers were used in the lower core, upper core, and cover. Those in the lower core were water cooled. The pressure in the pool was measured using a water-proof 3/8-inch-dia, four-element Tourmaline pressure transducer. The water surface displacement gages were conductivity probes. The high-speed camera recording the bubble expansion was a Hycam Model 41-004 at a nominal speed of 10,000 frames per second.

4. Discussion of Experiments and Results

4.1 Effects of Pressure Gradient

The nitrogen source experiments illuminate the dynamic features of the bubble expansion without the complications of heat transfer and phase change. Experiments were conducted with the internal structures present in various combinations. The experiments conducted and the results of these experiments are summarized in table 1. The nitrogen source was initially at 1450 psia and room temperature. A photo sequence from experiment D-002 with no internal structures is shown in fig. 5. In this experiment as the sliding doors separating the lower and upper cores begin to open, the nitrogen gas begins to accelerate the upper core and pool fluid. As this fluid begins to move, the thin viscous layer on the wall of the upper core is convected into the pool and rolls up into a vortex ring at the top of the upper core barrel. The bubble rising within the upper core contains a large volume of water with entrainments of about 80%. This entrainment is believed to result from the early instability of the accelerating gas-liquid interface and the associated mixing. As the bubble emerges into the coolant pool, it soon engulfs the vortex located just above the upper core. Although the percentage entrainment in the bubble falls (to $\sim$25% at slug impact) as the bubble expands, the entrained mass increases. This entrainment probably takes place at the sides of the bubble in association with the dissipating vortex. The axial bubble velocity is greater than the axial pool velocity, and the bubble grows radially until coolant slug impact. Slug impact occurs when the pool displaces the initial cover gas volume and impacts the vessel

Table 1

SUMMARY OF EXPERIMENTAL RESULTS, NITROGEN BUBBLE SOURCE

Exp. No.	Internal Structures Present	Initial Gap (inches)	Slug Impact Time (ms from doors begin to open)	Peak Cover Pressure[a] (psi)	Impulse of First Slug Impact Pulse (lbf-s)	Peak Surface Velocity[b] (in./ms)	Peak Slug Kinetic Energy[c] (kWs)
D-002	None	1.02	2.20	5310	67.0	1.12	3.24
D-006	None	0.91	2.16	4753	66.6	0.97	2.46
D-003	UCS Only	0.99	2.51	4095	59.4	0.97	2.42
D-005	UIS Only	0.90	2.75	2960	43.3 8.8 (UIS impulse)	0.59	0.85
D-004	UCS + UIS	0.81	2.84	2462	40.0	0.50	0.61

[a] Average value for each experiment.

[b] The value at slug impact of the derivative of a polynomial fit to the average water surface displacement gage measurement.

[c] Based on the peak surface velocity and the total mass of liquid contained in the pool above the top of the upper core.

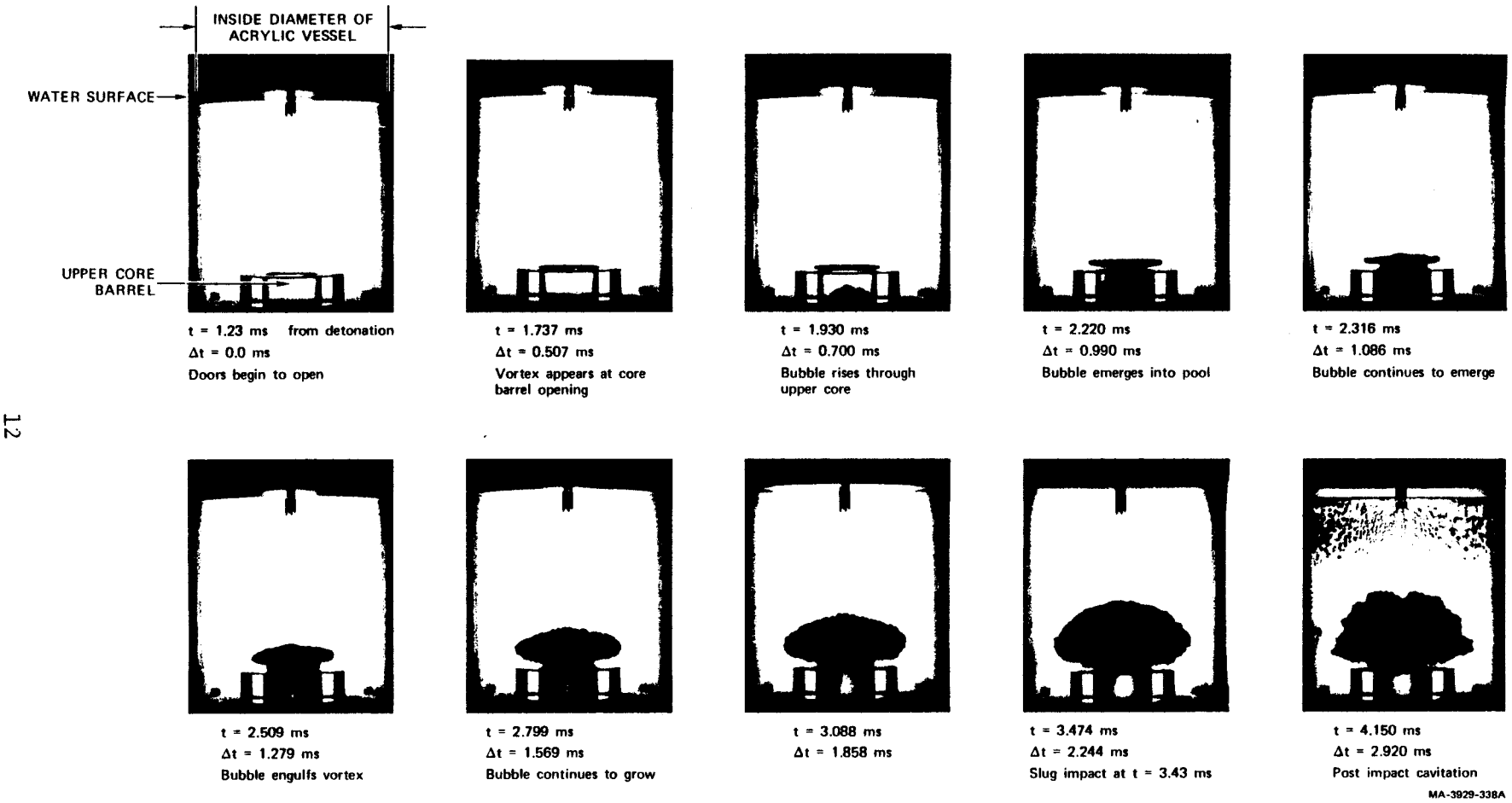

FIGURE 5 EXPERIMENT D-002 PHOTO SEQUENCE, NITROGEN BUBBLE SOURCE (NO INTERNAL STRUCTURES)

cover. A typical slug impact pressure record (fig. 6) shows several pulses, which occur as the water surface recoils off the vessel cover following slug impact and then reimpacts the cover as the core gas reexpands. The impulses shown in table 1 were calculated for the first impact pulse over an 0.8-ms interval beginning at a 90% compression of the cover gas.

During the expansion to slug impact, a pressure gradient exists between the lower core and the bubble within the pool. This gradient informs us that the expansion process is not quasi-static. The pressure doing the work on the coolant slug is the pressure acting at the gas-liquid interface of the expanding bubble which is lower than the pressure in the lower core. This interface is established as the sliding doors open and then moves past the upper core and bubble pressure transducers as the bubble expands. The pressure at this interface is determined from pressure records taken at specific locations within the apparatus. Fig. 7(a) shows lower core, upper core, and pool and bubble pressure measurements for the nitrogen source experiment with no internal structures. Those portions of these pressure records that best characterize the interface pressure are assembled into the composite shown in fig. 7(b).

The expansion work done by the source in driving the coolant pool upward until it impacted on the vessel cover (the integral of the product of the composite interface pressure and the differential volume displaced by the pool) was 2.98 kWs. This is approximately 66% of that expected in an ideal quasi-static expansion. The peak slug kinetic energy should approximate this work done on the slug by the bubble source if there are no significant energy losses and few turbulent or rotational motions.

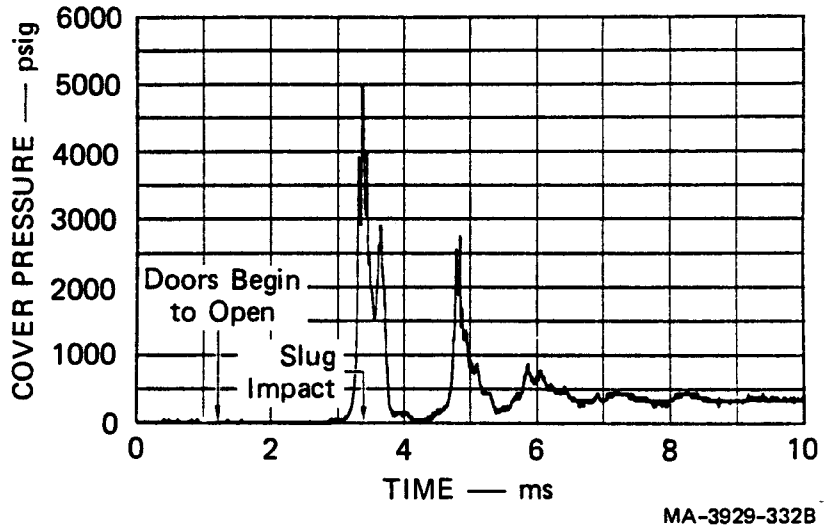

FIGURE 6 TYPICAL COVER PRESSURE, EXPERIMENT D-006 (NO INTERNAL STRUCTURES), NITROGEN BUBBLE SOURCE

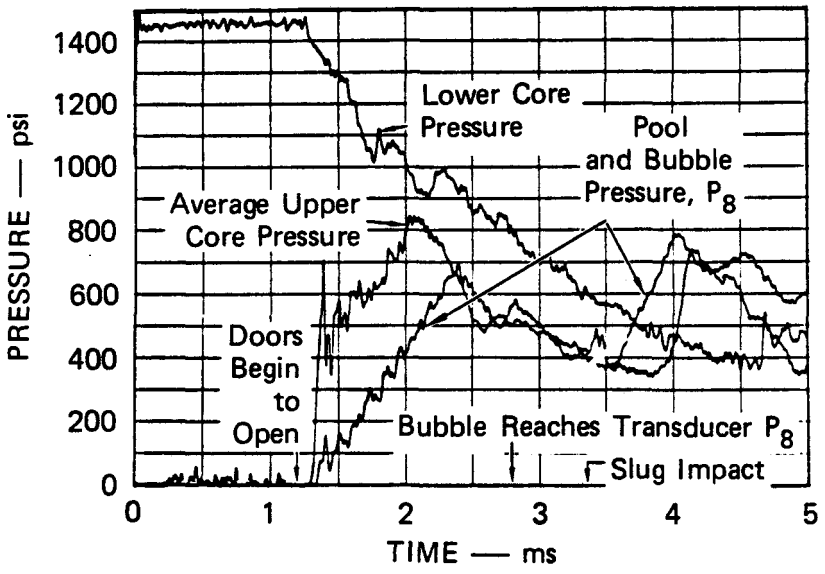

(a) VESSEL PRESSURES

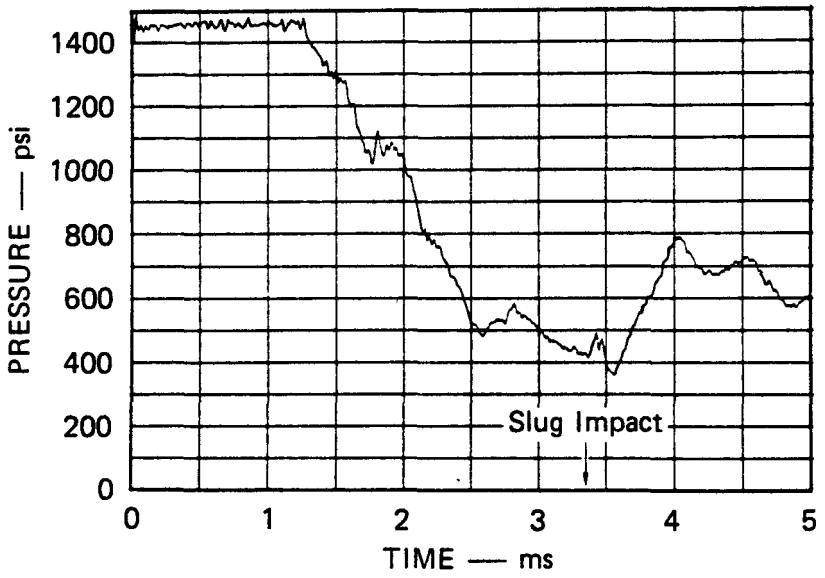

(b) BEST ESTIMATE OF THE PRESSURE ACTING AT THE GAS-LIQUID INTERFACE OF THE COOLANT SLUG

MA-3929-372B

FIGURE 7 PRESSURE ACTING AT THE BUBBLE INTERFACE OF THE COOLANT SLUG, EXPERIMENT D-006 (NO INTERNAL STRUCTURES), NITROGEN BUBBLE SOURCE

The peak kinetic energy of the slug can be estimated by assuming that all the coolant liquid above the top of the upper core moves at the velocity of the water surface. Support for this simple method of calculating the slug kinetic energy comes from predictions of these experiments made at Los Alamos Scientific Laboratory using the SIMMER II computer code [3]. The average value of the peak slug kinetic energy for experiments D-006 and D-002 is 2.85 kWs, which is within 4% of the expansion work done on the slug by the bubble source, as discussed above. Since the expansion work done by the source and the slug axial kinetic energy are about equal, we conclude that, in the absence of internal structures, the coolant slug moves with little energy loss or turbulence production in response to the work done on it by the bubble source, and the expansion work of the nitrogen source is attenuated solely due to the non-static nature of the expansion.

4.2 Effects of Internal Structures

The effects of fixed internal structures on the primary slug impact pulse are shown for both bubble sources in fig. 8(a) and (b). Internal structures attenuate the slug impact energy by increasing the time to slug impact, reducing the slug impact velocity, and reducing the peak pressure and impulse of the vessel cover. The upper core structure tested caused the smallest change in response, and the presence of both structures caused the greatest change. The apparent mechanisms that produce this result are throttling and the diversion of a portion of gas work from the production of axial motion to the production of organized rotational motion (in the

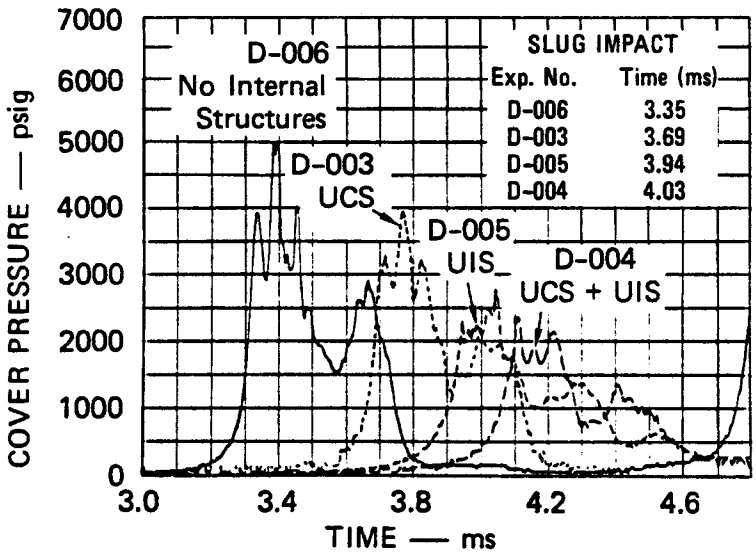

(a) NITROGEN BUBBLE SOURCE

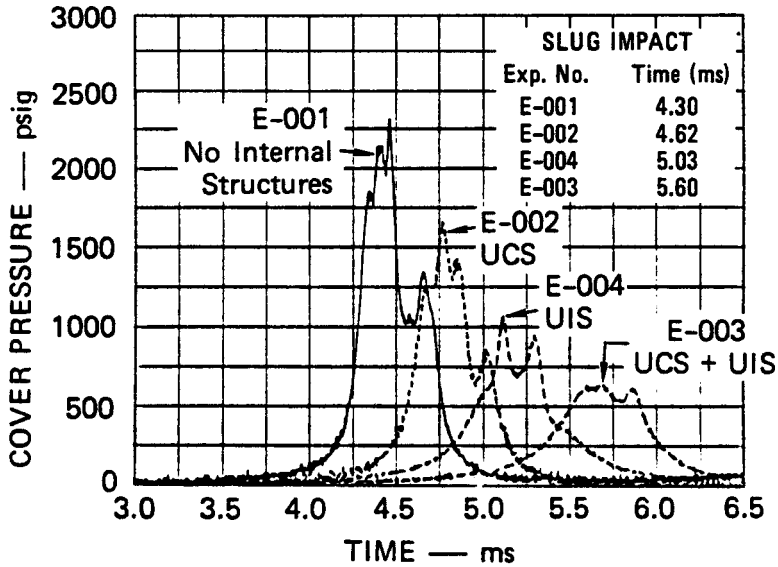

(b) FLASHING WATER BUBBLE SOURCE

MA-3929-314B

FIGURE 8 EFFECT OF INTERNAL STRUCTURES ON THE FIRST SLUG IMPACT PRESSURE PULSE

form of vortices) and random turbulent motion. The effects of internal structures on the peak pool surface velocity, peak slug kinetic energy, peak cover pressure, and slug impact impulse are summarized for both bubble sources in table 2.

4.3 Nonequilibrium Effects

The flashing water source experiments were more complex than the nitrogen source experiments because of the presence of heat transfer and phase change phenomena. Experiments were conducted with the same combinations of internal structures that were studied with the nitrogen source. The flashing source contained saturated liquid at initial conditions of 1160 psia and 563°F. Results from the flashing source experiments are summarized in table 3. A typical slug impact pressure record is shown in fig. 9. The impulses shown in table 3 were calculated for the first slug impulse pulse over a 1.0-ms interval beginning at a 90% compression of the cover gas. The experiment without internal structures proceeded in a manner quite similar to that described above for the nitrogen source. However, pressure histories in the lower core, upper core, and bubble were of a different character.

Pressure records typical of the flashing source experiment with no internal structures are shown in fig. 10(a). An explanation of the character of the lower core pressure record typical of the flashing source is found in nonequilibrium thermodynamics. When the sliding doors are opened, an expansion wave travels into the lower core and reduces the pressure.

Table 2

SUMMARY OF THE EFFECTS OF INTERNAL VESSEL STRUCTURES

INTERNAL STRUCTURE(S)	REDUCTION COMPARED WITH NO INTERNAL STRUCTURES			
	Peak Surface Velocity	Peak Slug Kinetic Energy	Peak Cover Pressure	Slug Impact Impulse
Nitrogen Bubble Source				
UCS[a] Only	7%	15%	19%	11%
UIS[b] Only	44%	70%	41%	35%[c] 22%[d]
Both UCS + UIS	52%	79%	51%	40% 27%
Flashing Water Bubble Source				
UCS Only	7%	15%	28%	22%
UIS Only	37%	63%	54%	42% 11%
Both UCS + UIS	45%	74%	71%	56% 25%

[a] Upper Core Structure.

[b] Upper Internal Structure.

[c] Impulse based on the slug impact pressure.

[d] Impulse based on the slug impact pressure and the additional load applied to the cover through the UIS columns.

Table 3

SUMMARY OF EXPERIMENTAL RESULTS, FLASHING WATER BUBBLE SOURCE

Exp. No.	Internal Structures Present	Initial Gap (inch)	Slug Impact Time (ms from doors begin to open)	Peak Cover Pressure[a] (psi)	Impulse of First Slug Impact Pulse (lbf-s)	Peak Surface Velocity[b] (in./ms)	Peak Slug Kinetic Energy[c] (kWs)
E-001	None	0.89	3.10	2325	41.9	0.67	1.26
E-002	UCS Only	0.90	3.43	1667	32.5	0.62	1.07
E-004	UIS Only	0.91	3.86	1082	24.3 13.2 (UIS impulse)[d]	0.42	0.46
E-003	UCS + UIS	0.92	4.41	668	18.3 13.2 (UIS impulse)[d]	0.37	0.33

[a] Average value for each experiment.

[b] The value at slug impact of the derivative of a polynomial fit to the average water surface displacement gage measurement.

[c] Based on the peak surface velocity and the total mass of liquid contained in the pool above the top of the upper core.

[d] Composite based on Experiments E-003 and E-004.

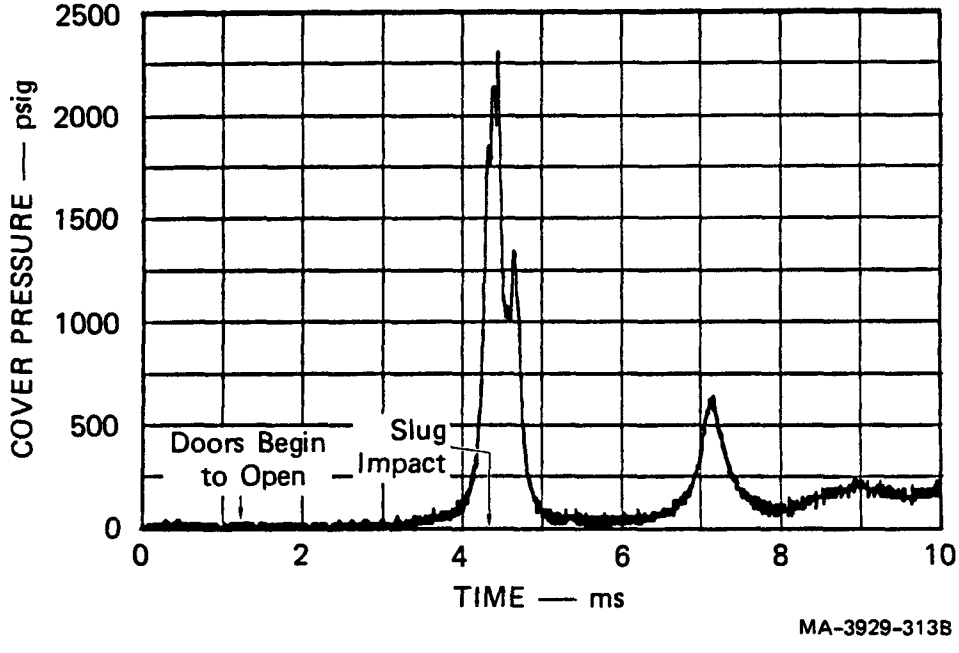

FIGURE 9 TYPICAL COVER PRESSURE, EXPERIMENT E-001 (NO INTERNAL STRUCTURES), FLASHING WATER BUBBLE SOURCE

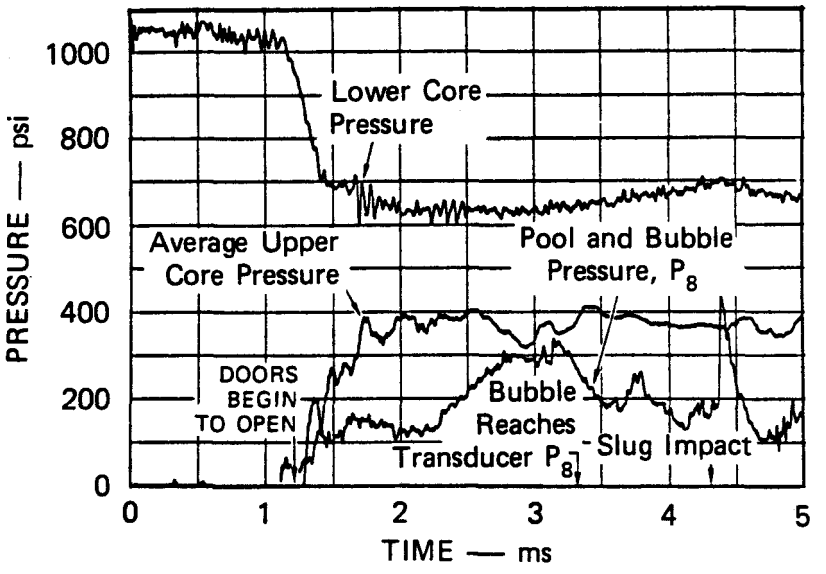

(a) VESSEL PRESSURES

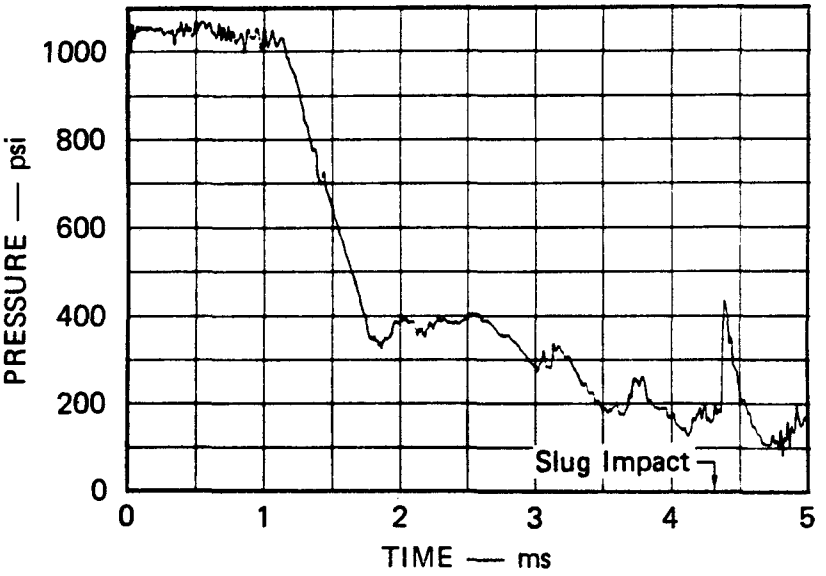

(b) BEST ESTIMATE OF THE PRESSURE ACTING AT THE VAPOR-LIQUID INTERFACE OF THE COOLANT SLUG

MA-3929-373B

FIGURE 10 PRESSURE ACTING AT THE BUBBLE INTERFACE OF THE COOLANT SLUG, EXPERIMENTS E-001 AND C-007 (NO INTERNAL STRUCTURES), FLASHING WATER BUBBLE SOURCE

This reduction in pressure supersaturates the lower core liquid, resulting in a metastable state, and vapor formation begins in an attempt to restore equilibrium. Formation of vapor bubbles requires that heat be extracted from the liquid adjacent to the bubble and invested as heat of vaporization in the forming vapor. Thus, the vapor and adjacent liquid are cooler than the bulk liquid, and a thermal nonequilibrium exists. The pressure in the flashing liquid drops to the saturation pressure corresponding to the bubble vapor temperature.

The 1/30-scale flashing water expansions are not equilibrium expansions because the time for expansion, τ, is short compared with the time for the temperature and pressure of the water to reach equilibrium, t_r, i.e., $\tau/t_r \ll 1$. Therefore, the nonequilibrium effects observed in the 1/30-scale experiments would be expected to occur at full-scale if the ratio τ/t_r is also less than one at full scale. The actual value of τ/t_r in either small- or large-scale experiments will determine the fraction of the equilibrium work that is done in moving the coolant slug. It is, therefore, the equilibrium, or "relaxation," time (t_r) that we need to be able to predict analytically or measure experimentally before we can predict the behavior of expansions of prototypic materials at full scale. This relaxation time depends on both the physical properties of the flashing liquid and the geometrical distribution of the liquid and solid surfaces in contact with it. Experimental support for a nonequilibrium expansion model would provide a strong basis for the understanding and choice of a prototypic source

simulant material. Because the nonequilibrium nature of the flashing source expansion results in a lower core pressure below the pressure that would occur during an equilibrium expansion, the source expansion work is less than the ideal work potential of the flashing source.

As in the nitrogen experiments, a pressure gradient exists between the lower core and the bubble within the pool; therefore, the pressure acting on the coolant slug is not well represented by the lower core pressure. This gradient may be due to unsteady or two-phase phenomena such as choking in the flow path between the lower core and the pool. The pressure acting on the coolant slug is estimated to be that shown in fig. 10(b).

The expansion history of the flashing water source is presented in fig. 11. Three curves are shown representing (1) an ideal expansion of the water based on a constant energy expansion into the volume created by the sliding door motion and an isentropic expansion into the volume created by the motion of the coolant slug, (2) the expansion history based on the lower core pressure, and (3) the expansion history based on the estimated pressure acting on the coolant. That portion of the area under these curves not associated with the constant energy expansion into the volume created by the sliding door motion is the work done in the expansion. The lower core pressure curve demonstrates an attenuation of the source work potential due to nonequilibrium phenomena in the flashing water. The expansion work calculated using the coolant slug pressure

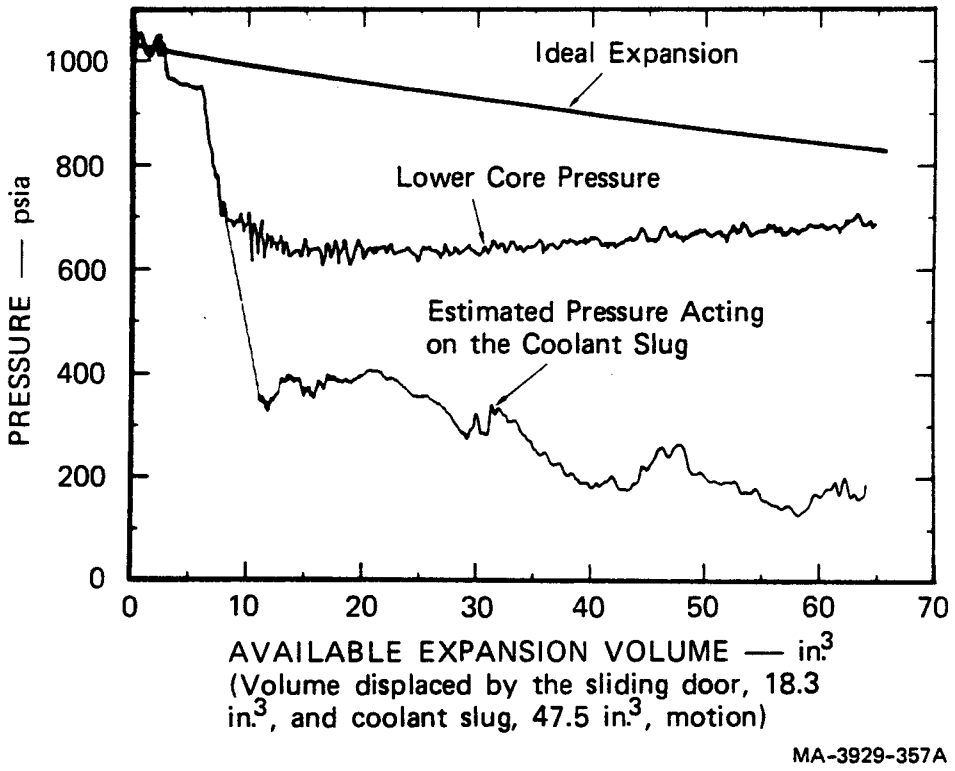

FIGURE 11 EXPANSION OF THE FLASHING WATER BUBBLE SOURCE, EXPERIMENT E-001 (NO INTERNAL STRUCTURES)

demonstrates an attenuation of the source work potential because of the two attenuation mechanisms: (1) the 400-psi or 40% reduction in lower core pressure due to nonequilibrium effects and (2) the further 300-psi or 50% reduction due to the pressure gradient between the lower core and the gas-liquid interface of the expanding bubble. The calculated expansion work done by the source in driving the coolant pool upward until it impacted the vessel cover was 1.3 kWs. This is approximately 25% of that expected in an ideal quasi-static expansion and compares with a peak slug kinetic energy of 1.26 kWs based on the assumption that all the liquid above the top of the upper core is moving at the coolant water surface velocity.

4.4 Scaling Considerations

A scaling analysis (table 4) of the nitrogen source experiments, based on the significant physical parameters, was conducted. Our concern was whether the dynamic phenomena present in a nitrogen source experiment at 1/30-scale would be present to the same degree in a full-scale experiment using the same materials and initial conditions. This includes such features as the bubble shape, the percentage entrainment in the upper core and bubble, and the slug impact pressure. If all of these features are present ot the same degree at 1/30- and full-scales, then the attenuation of the expansion work potential due to the pressure gradient and internal structures will scale.

The only dimensionless parameters that have different values at 1/30- and full-scale are the Reynolds and Weber numbers. Since both of

Table 4

NITROGEN SOURCE EXPERIMENT SCALING ANALYSIS

INDEPENDENT PARAMETER	MODEL/FULL-SCALE
System Lengths	1/30
Bubble Source Material	Same at either scale
Upper Core and Pool Material	Same at either scale
Cover Gas Material	Same at either scale
Initial Conditions (p, T, etc.)	1/1

COMPLETE SET OF CHARACTERISTIC PARAMETERS	
Length, L	1/30
Pressure, P	1/1
Density, ρ	1/1
Sound Speed, c	1/1
Surface Tension, σ	1/1
Kinematic Viscosity, ν	1/1
Acceleration, $a \sim \frac{P}{\rho L}$	30/1
Time, $\tau \sim \sqrt{L/a}$	1/30
Velocity, $V \sim at$	1/1

COMPLETE SET OF DIMENSIONLESS PARAMETERS	
t/τ — Time/Characteristic Time	1/1
v/V — Velocity/Characteristic Velocity	1/1
p/P — Pressure/Characteristic Pressure	1/1
V/c (Mach No.) — Velocity/Sound Speed	1/1
VL/ν (Reynolds No.) — Inertia Force/Viscous Force	1/30
$\rho V^2 L/\sigma$ (Weber No.) — Inertia Force/Surface Tension Force	1/30

these dimensionless numbers are large at either scale, viscous and surface tension forces will play a small role and hence do not have a significant influence on the macroscopic dynamic features of the bubble expansion. Therefore, the physical features of and expansion work attenuation in the nitrogen experiments will scale.

The behavior of flashing source experiments at full-scale is not completely understood because of questions about the nonequilibrium and two-phase phenomena present in the 1/30-scale flashing source experiments. Experiments are in progress at SRI International to address these questions and to identify other simulant materials that might behave in a manner more typical of the core materials in a prototype LMFBR.

5. Conclusions

Three physical mechanisms that attenuate the work potential of the expanding bubble source have been described: (1) the unsteady core material expansion, (2) the restrictions to the expansion by internal structures, and (3) nonequilibrium effects in the flashing liquid source. These effects are summarized in table 5. The nitrogen expansion without internal structures demonstrates a 34% attenuation due to unsteady expansion effects. The flashing water expansion without internal structures demonstrates a 76% attenuation due to unsteady and nonequilibrium effects. In the flashing water expansion with structures present, the three attenuation mechanisms combined to result in a 95% reduction in the flashing water work potential.

Table 5

AXIAL SLUG KINETIC ENERGY
AS A PERCENTAGE OF THE IDEAL QUASI-STATIC
WORK POTENTIAL OF THE BUBBLE SOURCE

Bubble Source	Without Internal Structures	With Upper Core and Upper Internal Structures
Nitrogen	66%	14%
Flashing water	24%	5%

These results demonstrate the importance of dynamic phenomena in attenuating the expansion work potential in qualitatively simulated HCDAs and should help in verifying models used in SIMMER II and other codes for predicting the work potential of HCDAs in prototype LMFBRs. The hydrodynamic features of these experiments will be important in full-scale HCDAs. The thermodynamic and nonequilibrium phenomena may differ in the prototype due to the different temperature regime and material properties.

6. Future Work

Future work is being conducted at SRI to address the scaling of thermodynamic and nonequilibrium phenomena. We are extending the scaling analysis of the hydrodynamic phenomena mentioned here to include heat transfer and phase change phenomena. Experiments to study nonequilibrium phenomena in flashing liquids are currently in progress.

Acknowledgements

These experiments were conducted during the period September 1977 to April 1978 under the support of the U.S. Department of Energy, Contract EY-76-C-03-0115. We wish to thank Dale W. Ploeger, who conducted many of these experiments and who developed the flashing source and sliding door systems, and Robert W. Blomenkamp, who designed and made operational the experiment instrumentation.

References

[1] R. J. Tobin and D. J. Cagliostro, Effects of Vessel Internal Structures on Simulated HCDA Bubble Expansion, Technical Report 5, SRI Project PYU-3929, SRI International, Menlo Park, CA (November 1978).

[2] D. J. Cagliostro, A. L. Florence, G. R. Abrahamson, and G. Nagumo, Characterization of an Energy Source for Modeling Hypothetical Core Disruptive Accidents in Nuclear Reactors, Nucl. Eng. Des. Vol. 27, No. 1 (1974).

[3] C. R. Bell, et al., SIMMER-II Analysis of LMFBR Post-Disassembly Expansion, Proceedings of the ENS/ANS International Topical Meeting on Nuclear Power Reactor Safety, Brussels, Belgium, 16-19 October 1978.

ILLUSTRATIONS

TABLES